

# Self-referencing circular dichroism ion yield measurements for improved statistics using femtosecond laser pulses

Cite as: Rev. Sci. Instrum. 92, 033001 (2021); doi: 10.1063/5.0036344

Submitted: 4 November 2020 • Accepted: 18 February 2021 •

Published Online: 10 March 2021



View Online



Export Citation



CrossMark

T. Ring, C. Witte, S. Vasudevan,  S. Das, S. T. Ranecky, H. Lee, N. Ladda, A. Senftleben,  H. Braun, <sup>a)</sup>  and T. Baumert 

## AFFILIATIONS

Universität Kassel, Heinrich-Plett-Str. 40, 34132 Kassel, Germany

<sup>a)</sup> Author to whom correspondence should be addressed: braun@physik.uni-kassel.de. URL: <https://www.uni-kassel.de/exp3>

## ABSTRACT

The combination of circular dichroism with laser mass spectrometry via the measurement of ion yields is a powerful tool in chiral recognition, but the measured anisotropies are generally weak. The method presented in this contribution reduces the measurement error significantly. A common path optical setup generates a pair of counter-rotating laser foci in the interaction region of a time-of-flight spectrometer. As the space focus condition is fulfilled for both foci individually, this becomes a twin-peak ion source with well separated and sufficiently resolved mass peaks. The individual control of polarization allows for *in situ* correction of experimental fluctuations measuring circular dichroism. Our robust optical setup produces reliable and reproducible results and is applicable for dispersion sensitive femtosecond laser pulses. In this contribution, we use 3-methyl-cyclopentanone as a prototype molecule to illustrate the evaluation procedure and the measurement principle.

© 2021 Author(s). All article content, except where otherwise noted, is licensed under a Creative Commons Attribution (CC BY) license (<http://creativecommons.org/licenses/by/4.0/>). <https://doi.org/10.1063/5.0036344>

## I. INTRODUCTION

Optical activity phenomena rely on the helicity-specific response of a substance to circularly polarized (cpl) light.<sup>1</sup> In this way, the enantiomers of chiral molecules can be distinguished via light-matter interaction. One example is circular dichroism (CD), which is defined as the difference in extinction of left and right circularly polarized (lcp and rcp, respectively) light. While absorption CD is well established in the liquid phase,<sup>2</sup> emerging gas phase techniques<sup>3,4</sup> allow for collision and interaction free measurements and yield signals from small amounts of sample. The direct transfer to low pressure absorption CD measurements triggered the development of cavity-enhanced polarimetry with a Fabry-Perot<sup>5</sup> or cavity ring down<sup>6</sup> approach. Instead, the CD of an optically active electronic resonance can also be mapped to the ionization continuum by resonance enhanced multi-photon ionization (REMPI).<sup>7,8</sup> The combination with time-of-flight laser mass spectrometry (LaMS) allows for the detection of the CD of parent and fragment ions, and measurements have been reported on a variety of chiral molecules.<sup>9-11</sup>

A strong differential photoion circular dichroism has been reported recently.<sup>12</sup> The determination of the CD in the ion yield can be used to discriminate between different conformers of a chiral species,<sup>11</sup> and the component resolved analysis of mixtures of different molecules can be envisioned. The integrated ion yield  $I_{lcp}$  ( $I_{rcp}$ ) after ionization with left (right) circularly polarized light reflects the helicity dependent interaction of chiral molecules. The normalized difference is called anisotropy  $g$  and has proved to be equal to the normalized CD in extinction  $\epsilon$  for a specific resonance,<sup>9</sup>

$$g = 2 \cdot \frac{\epsilon_{lcp} - \epsilon_{rcp}}{\epsilon_{lcp} + \epsilon_{rcp}} = 2 \cdot \frac{I_{lcp} - I_{rcp}}{I_{lcp} + I_{rcp}}. \quad (1)$$

If more resonances are involved, each of them contributes to the total anisotropy, which makes it a non-linear chiral effect like other well-known phenomena.<sup>13</sup> The accumulated effect is mirror symmetric with respect to the exchange of enantiomers.

In contrast to the angular resolved photoelectron CD,<sup>14,15</sup> which is based on electric dipole interactions, ion CD in absorption

is usually quite weak.<sup>16</sup> The magnitude of CD in ion yield is determined by the interplay of magnetic and electric dipole transitions: The largest effect is expected for (anti-) parallel dipole moments of the same size.<sup>17</sup> This makes the electric dipole forbidden carbonyl  $\pi^* \leftarrow n$  transition<sup>18,19</sup> a prominent candidate for CD measurements. In the case of 3-methyl-cyclopentanone (3-MCP), for example, the conjunction of narrow bandwidth nanosecond laser pulses and cold molecules resulted in anisotropies of more than 40% for distinct vibrational resonances.<sup>20</sup> In general, photoelectron CD and CD in ion yield strongly depend on the wavelength<sup>21–23</sup> and it is *a priori* not clear which technique will lead to larger effects and thereby offer better discrimination between the enantiomers.<sup>24</sup>

A complementary approach to narrow band nanosecond excitation is the use of broadband femtosecond laser pulses.<sup>25</sup> The shorter pulse duration allows us to probe molecular dynamics, and cumulative series of resonances may be addressed. To enhance the sensitivity of LaMS-CD, the use of achiral reference substances and a self-referencing twin-peak approach have proved useful.<sup>9</sup> In this contribution, we present a common path twin-peak setup that accounts for the crucial point of dispersion management in the context of femtosecond laser pulses.

## II. SET-UP AND DATA ANALYSIS

The setup is depicted in Fig. 1(a). A titanium–sapphire amplifier (Femtopower HE 3 kHz) generates 25 fs short laser pulses at a central wavelength of 785 nm and a pulse energy of 1.6 mJ. Around 400  $\mu$ J are used to pump a tunable optical parametric amplifier system (TOPAS by Light Conversion), which can be tuned from UV to near infrared including harmonic generation. The output of this light source is focused ( $f = 50$  cm) into a linear two-stage time-of-flight spectrometer, perpendicular to an effusive molecular beam. An alkali dispenser provides additional potassium vapor as the achiral reference. In this contribution, experiments are performed at 309 nm and 322 nm with bandwidth limited pulses with a full width at half maximum duration of less than 40 fs. A pulse energy of 0.7  $\mu$ J is focused down to a spot size with a  $1/e^2$  diameter of 90  $\mu$ m, which results in an intensity of  $5 \times 10^{11}$  W/cm<sup>2</sup>.

The ions generated in the interaction region are accelerated toward a multi-channel-plate detector (APTOF40 by Photonis) and the signal is recorded without further amplification using a Waverunner 640Zi (Teledyne LeCroy) oscilloscope. Typically, 1280 consecutive laser shots are averaged to obtain time-of-flight spectra with a good signal-to-noise ratio and to perform chiral analysis as follows:

The goal of the presented twin-peak method is a self-referencing measurement of circular dichroism in a robust and reproducible manner. Therefore, the space focus of a Wiley–McLaren electrode configuration<sup>26</sup> that enhances the mass resolution for an extended interaction region is deliberately detuned to map ions created at two separate points of ionization with a specific time delay onto the detector.<sup>27</sup> The time delay results in the appearance of two peaks for each mass/charge ratio in the time-of-flight spectrum, hence the designation twin-peak. The common path optical setup creates the required close-lying focal points. In detail, a half-wave plate first rotates the plane of polarization of the incoming laser beam to 45°. Consequently, the Wollaston prism (opening angle  $\alpha = 10^\circ$ , Bernhard Halle) splits up the incoming beam into two

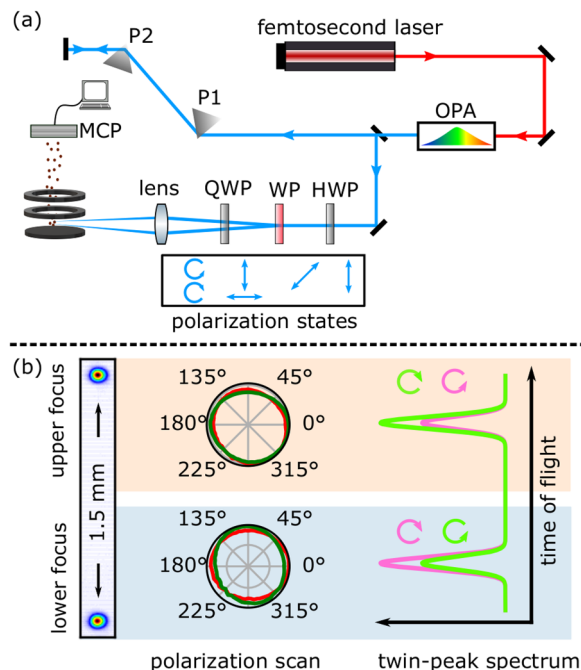


**FIG. 1.** Setup: (a) the near-infrared pulses are converted to UV light pulses using the optical parametric amplifier. The prisms (P1 and P2) are used for dispersion management. The common path optical setup generates two beams of opposite helicity: A half-wave plate (HWP) rotates the polarization such that the Wollaston prism (WP) splits up the beam into two divergent beams of perpendicular polarization. These are converted to cpl light with a quarter-wave plate (QWP) and both are focused by a lens into the interaction region of the home-built time-of-flight spectrometer. (b) Image of the twin-peak foci taken with a beam profiling camera and the corresponding characterization of polarization for lcp (red curve) and rcp (green curve) light determined individually for both beams. The ion signals of a chiral molecule with enantiomeric excess resulting from the two positions are shown schematically (pink and light green). Rotating the QWP position from 45° to 135° exchanges the helicity between the upper and lower focus.

divergent beams of perpendicular polarization. Passing a lens, we obtain beam profiles in the focal area like those depicted in Fig. 1(b). Circular polarization with opposite helicity for both beams is generated with an achromatic quarter-wave plate and ensured by polarization scans in the overlap as well as for the individual beams. The latter are shown next to the beam profile measurements. Stokes S3 is well above 98% in all measurements presented in this contribution. The same optical path for both beams allows for simultaneous optical dispersion management for both foci. Specifically, we maximize the non-linear ionization signal of xenon by adjusting the prisms P1 and P2 [cf. Fig. 1(a)], thereby ensuring short pulses for both foci in the interaction region.

The anisotropy  $g$  can now be calculated within each recorded time-of-flight spectrum according to Eq. (1). The signals from the separate foci that result from ionization by left and right circularly polarized light are analyzed. Due to this simultaneous acquisition of the integrated ion yields  $I_{lcp}$  and  $I_{rcp}$ , slow or sudden fluctuation of the laser or pressure does not distort the measurement. To correct for systematic deviations of both foci, their helicity is inverted by rotating the quarter-wave plate between 45° and 135°, as depicted in

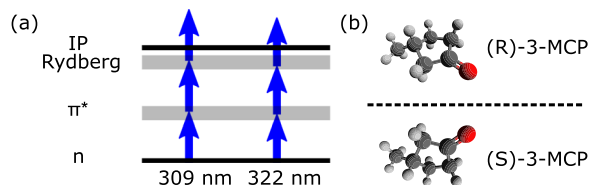
Fig. 1(b) in pink and green—the average of the anisotropies of both wave-plate positions is called twin-peak anisotropy. As an additional correction, the achiral reference potassium is evaluated accordingly. Any anisotropy measured for this achiral substance must be due to systematic errors and can be directly subtracted from the anisotropy calculated for the chiral sample.

### III. RESULTS

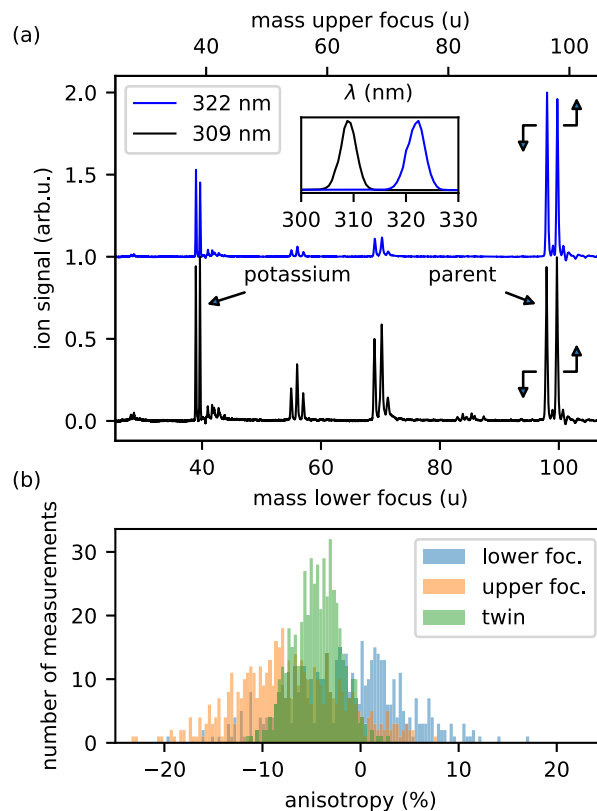
The monocyclic ketone 3-MCP [ $\text{CH}_3\text{C}_5\text{H}_7=\text{O}$ , both enantiomers are visualized in Fig. 2(b)] is known to show a large CD in absorption measurements. In addition, its high vapor pressure makes it suitable for gas phase experiments. Besides, its applicability in various measurements of CD in ion yield has been reported.<sup>8,20,28,29</sup> Here, we drive the  $\pi^* \leftarrow n$  transition with one photon in the near UV. Within this resonance, the absorption and the circular dichroism spectrum show three characteristic maxima.<sup>30</sup> The ionization is driven as a  $1 + 1 + 1$  resonance enhanced multi-photon ionization process via a Rydberg state as the second intermediate<sup>28</sup> [cf. Fig. 2(a)]. According to the maxima in anisotropy derived by a wavelength scan with femtosecond laser pulses, we present data for 309 nm and 322 nm. The third resonance at roughly 300 nm is not covered by our current measurement.

Figure 3(a) displays the twin-peak mass spectra for 309 nm (black) and 322 nm (blue). In each case, the left peaks correspond to the lower focus and the right peaks correspond to the upper one. The mass calibration is done independently for both laser foci. Note that the fragmentation pattern is strongly wavelength dependent—for shorter wavelengths, the predominance of the parent ion decreases especially in favor of the  $m = 69$  u fragment. The ratio of potassium and 3-MCP signal strength is adjusted for each setting individually to obtain similar ion signals. The difference in peak height for potassium resembles a measurement offset and shows the importance of achiral correction.

The twin peaks are well separated and sufficiently resolved. The mass spectrum of the lower focus is shifted to shorter flight times. For the parent ion ( $m = 98$  u), this mass dependent shift corresponds to a mass difference of 1.2 u compared to a full width at half maximum of  $\Delta m = 0.3$  u for the individual peaks. To avoid overlapping of peaks of close lying fragments or mixtures of substances and to adapt the procedure for heavier or lighter molecules, we can change the separation in ion-flight time by modifying the focal separation. The distance of the two foci (here  $\approx 1.5$  mm) is in first approximation determined only by the focal distance and the opening angle of the Wollaston prism. Robustness and reproducibility of the focus conditions can be ensured likewise.



**FIG. 2.** (a) Schematic representation of the  $1+1+1$  resonance enhanced multi-photon ionization of 3-MCP. The excitation paths for both 309 nm and 322 nm include the same electronic resonances but different vibrational levels (not depicted). (b) Visualization of both enantiomers in ball-and-stick representation.



**FIG. 3.** (a) Twin-peak spectrum of (S)-3-MCP and potassium at 322 nm (blue line, lifted by an offset of 1 arb.u.) and 309 nm taken with circularly polarized light (average of lcp and rcp ionization). The inset shows the corresponding laser spectra with a full width at half maximum bandwidth of  $\Delta\lambda_{309} = 3.6$  nm and  $\Delta\lambda_{322} = 4.0$  nm. The bottom axis corresponds to the lower focus (left one of the twin peaks), and the top axis corresponds to the upper focus. (b) Statistical distribution of 500 consecutive measurements of twin-peak anisotropy for (S)-3-MCP with bandwidth limited pulses at 309 nm (green histogram). In addition, the lower and upper foci have been evaluated single-peak wise to highlight the impact of the self-referencing principle (blue and orange histogram). The histograms display three bars per 1% anisotropy.

For chiral discrimination, the potassium corrected twin-peak anisotropy is determined, as described in Sec. II. The green histogram in Fig. 3(b) displays the statistical distribution of 500 of these measurements of (S)-3-MCP. The mean of this distribution is  $(-4.4 \pm 0.3)\%$  where the error is defined as the statistical  $3\sigma$  interval of the mean (see the [supplementary material](#)). To emphasize the added value of the twin-peak principle, the ion signal of both foci is evaluated individually, which is equivalent to single focus measurements. Here, the absolute error is 0.7% in both cases. The significantly reduced statistical noise for the twin-peak evaluation [cf. width of orange/blue vs green distribution in Fig. 3(b)] can be attributed to the correction of laser fluctuations (position/intensity) or changes in the gas pressure. In addition, the twin-peak procedure corrects for systematic offsets occurring in the single-peak measurement. The latter occur mainly due to changes in the beam characteristics while changing the position of the quarter-wave plate. A detailed discussion of the statistical behavior and error correction is

**TABLE I.** Twin-peak anisotropies for bandwidth limited pulses at 309 nm and 322 nm. The results are corrected with potassium as an achiral reference substance.

$\lambda$ (nm)	(R)-3-MCP (%)	(rac)-3-MCP (%)	(S)-3-MCP (%)
309	$(4.1 \pm 0.6)$	$(-0.2 \pm 0.6)$	$(-4.4 \pm 0.3)$
322	$(1.1 \pm 0.6)$	$(0.2 \pm 0.5)$	$(-1.0 \pm 0.6)$

given in the [supplementary material](#). Especially, in the case of much lower anisotropy factors, the significantly reduced error becomes important and might facilitate assignments between theoretical and experimental data.<sup>31,32</sup>

Table I displays the results for both enantiomers and the racemic mixture, measured at the two resonances using bandwidth limited pulses. Exchanging the enantiomer mirrors the chiral response and the CD of the racemate is centered around zero (see also the [supplementary material](#)). Like PECD experiments, for enantiomeric excess (ee) determination<sup>33,34</sup> it is, in principle, possible to measure ee via the CD in ion yield. It will, however, require the recording of calibration points to provide absolute values. Concise and accurate ee studies to this end are yet to be performed. In the case of our femtosecond measurements, the anisotropy at 309 nm is four times stronger than that at 322 nm. This ratio is contradictory to the CD in absorption for the  $\pi^* \leftarrow n$  transition. A lower anisotropy means either less pronounced CD or stronger absorption. In comparison to the single photon absorption CD, also the second resonance [cf. Fig. 2(a)] contributes to the final value. It is well-known that the first resonance ( $\pi^* \leftarrow n$ ) is modulated with wavelength in absorption as well as in CD,<sup>30</sup> and the same can be expected for the Rydberg intermediate.<sup>18</sup> The influence onto broadband excitation with femtosecond laser pulses is not obvious, but other measurements with femtosecond laser pulses confirm the observed trends: The lower resonance shows an anisotropy of 6.5% at 308.3 nm and 6.0% at 311 nm, and the upper one shows an anisotropy of 2.0% (321.7 nm), 1.8% (322.9 nm), and 2.6% (325 nm).<sup>25</sup> LaMS-CD measurements with nanosecond laser pulses result in a maximum of anisotropy of 27% at 324 nm.<sup>23</sup> The higher peak intensity of the femtosecond laser pulses (in comparison to nanosecond laser pulses) might play a role. This is closely related to the decrease in  $g$  for shorter laser pulse duration.<sup>35</sup>

Moreover, the wavelength dependence of this effect and the different transition moments for the vibrational levels can result in an (as of yet) unintentional accumulation of anisotropies. Especially, in the superposition of more than one electronic resonance in multi-photon excitation, the interpretation becomes challenging.<sup>36</sup> This causes the difficulty to predict the maximal anisotropy to be measured with femtosecond laser pulses of a certain bandwidth. On the other hand, this behavior promises great opportunities for controlled accumulation of resonances. Pulse shaping has the potential to enhance this type of chiral recognition and eventually enable coherent control<sup>37,38</sup> (and references therein) of chiroptical signals with respect to enhanced enantioselectivity also in mixtures.

#### IV. SUMMARY

In this contribution, we present a common path optical setup to perform self-referencing CD measurements in ion yield with femtosecond laser pulses. In this way, we can correct for experimental

fluctuations and bias *in situ*. The chiral molecule 3-MCP serves as a prototype to present the data evaluation procedure and the functionality of the method. It proves to be robust and reliable. The common path setup allows for optical dispersion management, which is crucial in femtosecond spectroscopy. The resulting ability to combine pulse shaping with CD measurements may open up a path to coherent control of chiral systems.

#### SUPPLEMENTARY MATERIAL

See the [supplementary material](#) for the description of the evaluation procedure to determine the twin-peak anisotropy  $g$  in detail on the example of racemic 3-MCP and discussion on the statistical behavior and error correction.

#### ACKNOWLEDGMENTS

This work was funded by the Deutsche Forschungsgemeinschaft (DFG, German Research Foundation)—Project No. 328961117—SFB 1319 ELCH. The authors thank Christian Lux for his pioneering work in this project.

#### DATA AVAILABILITY

The data that support the findings of this study are available from the corresponding author upon reasonable request.

#### REFERENCES

- 1 L. D. Barron, *Molecular Light Scattering and Optical Activity* (University Press, Cambridge, 2004), Vol. 2.
- 2 *Circular Dichroism: Principles and Applications*, edited by N. Berova, K. Nakanishi, and R. W. Woody (Wiley VCH, New York; Chichester; Weinheim; Brisbane; Singapore; Toronto, 2000).
- 3 *Chiral Recognition in the Gas Phase*, edited by A. Zehner (CRC Press, Boca Raton, FL, 2010).
- 4 D. Patterson and M. Schnell, "New studies on molecular chirality in the gas phase: Enantiomer differentiation and determination of enantiomeric excess," *Phys. Chem. Chem. Phys.* **16**, 11114–11123 (2014).
- 5 J. Poirson, M. Vallet, F. Bretenaker, A. Le Floch, and J. Y. Thépot, "Resonant cavity gas-phase polarimeter," *Anal. Chem.* **70**, 4636–4639 (1998).
- 6 T. Müller, K. B. Wiberg, and P. H. Vaccaro, "Cavity ring-down polarimetry (CRDP): A new scheme for probing circular birefringence and circular dichroism in the gas phase," *J. Phys. Chem. A* **104**, 5959–5968 (2000).
- 7 U. Boesl von Grafenstein and A. Bornschlegl, "Circular dichroism laser mass spectrometry: Differentiation of 3-methylcyclopentanone enantiomers," *ChemPhysChem* **7**, 2085–2087 (2006).
- 8 R. Li, R. Sullivan, W. Al-Basheer, R. M. Pagni, and R. N. Compton, "Linear and nonlinear circular dichroism of R-(+)-3-methylcyclopentanone," *J. Chem. Phys.* **125**, 144304 (2006).
- 9 U. Boesl, A. Bornschlegl, C. Logé, and K. Titze, "Resonance-enhanced multiphoton ionization with circularly polarized light: Chiral carbonyls," *Anal. Bioanal. Chem.* **405**, 6913–6924 (2013).
- 10 P. H. Horsch, G. Urbasch, and K.-M. Weitzel, "Circular dichroism in ion yield in multiphoton ionization of (R)-propylene oxide employing femtosecond laser pulses," *Z. Phys. Chem.* **225**, 587 (2011).
- 11 A. Hong, C. M. Choi, H. J. Eun, C. Jeong, J. Heo, and N. J. Kim, "Conformation-specific circular dichroism spectroscopy of cold, isolated chiral molecules," *Angew. Chem., Int. Ed.* **53**, 7805–7808 (2014).
- 12 K. Fehre, S. Eckart, M. Kunitski, C. Janke, D. Trabert, M. Hofmann, J. Rist, M. Weller, A. Hartung, L. P. H. Schmidt, T. Jahnke, H. Braun, T. Baumert,

- J. Stohner, P. V. Demekhin, M. S. Schöffler, and R. Dörner, "Strong differential photoion circular dichroism in strong-field ionization of chiral molecules," *Phys. Rev. Lett.* **126**, 083201 (2021).
- <sup>13</sup>P. Fischer and F. Hache, "Nonlinear optical spectroscopy of chiral molecules," *Chirality* **17**, 421–437 (2005).
- <sup>14</sup>B. Ritchie, "Theory of the angular distribution of photoelectrons ejected from optically active molecules and molecular negative ions," *Phys. Rev. A* **13**, 1411–1415 (1976).
- <sup>15</sup>N. Böwering, T. Lischke, B. Schmidtke, N. Müller, T. Khalil, and U. Heinzmann, "Asymmetry in photoelectron emission from chiral molecules induced by circularly polarized light," *Phys. Rev. Lett.* **86**, 1187–1190 (2001).
- <sup>16</sup>I. Powis, "Photoelectron spectroscopy and circular dichroism in chiral biomolecules: L-alanine," *J. Phys. Chem. A* **104**, 878–882 (2000).
- <sup>17</sup>P. M. L. Blok and H. P. J. M. Dekkers, "Discrimination between  $^3\pi\pi^*$  and  $^3n\pi^*$  states in organic-molecules by circular-polarization of phosphorescence," *Chem. Phys. Lett.* **161**, 188–194 (1989).
- <sup>18</sup>S. Feinleib and F. A. Bovey, "Vapour-phase vacuum-ultraviolet circular-dichroism spectrum of (+)-3-methylcyclopentanone," *Chem. Commun.* **16**, 978–979 (1968).
- <sup>19</sup>F. Pulm, J. Schramm, J. Hormes, S. Grimme, and S. D. Peyerimhoff, "Theoretical and experimental investigations of the electronic circular dichroism and absorption spectra of bicyclic ketones," *Chem. Phys.* **224**, 143–155 (1997).
- <sup>20</sup>K. Titze, T. Zollitsch, U. Heiz, and U. Boesl, "Laser mass spectrometry with circularly polarized light: Circular dichroism of cold molecules in a supersonic gas beam," *ChemPhysChem* **15**, 2762–2767 (2014).
- <sup>21</sup>A. Kastner, T. Ring, B. C. Krüger, G. B. Park, T. Schäfer, A. Senftleben, and T. Baumert, "Intermediate state dependence of the photoelectron circular dichroism of fenchone observed via femtosecond resonance-enhanced multi-photon ionization," *J. Chem. Phys.* **147**, 013926 (2017).
- <sup>22</sup>A. Kastner, G. Koumariou, P. Glodic, P. C. Samartzis, N. Ladda, S. T. Ranecky, T. Ring, S. Vasudevan, C. Witte, H. Braun, H.-G. Lee, A. Senftleben, R. Berger, G. B. Park, T. Schäfer, and T. Baumert, "High-resolution resonance-enhanced multiphoton photoelectron circular dichroism," *Phys. Chem. Chem. Phys.* **22**, 7404–7411 (2020).
- <sup>23</sup>C. Logé, A. Bornschlegl, and U. Boesl, "Progress in circular dichroism laser mass spectrometry," *Anal. Bioanal. Chem.* **395**, 1631–1639 (2009).
- <sup>24</sup>C. S. Lehmann and K.-M. Weitzel, "Coincident measurement of photo-ion circular dichroism and photo-electron circular dichroism," *Phys. Chem. Chem. Phys.* **22**, 13707–13712 (2020).
- <sup>25</sup>P. Horsch, G. Urbasch, and K.-M. Weitzel, "Analysis of chirality by femtosecond laser ionization mass spectrometry," *Chirality* **24**, 684–690 (2012).
- <sup>26</sup>W. C. Wiley and I. H. McLaren, "Time-of-flight mass spectrometer with improved resolution," *Rev. Sci. Instrum.* **26**, 1150–1157 (1955).
- <sup>27</sup>C. Logé, A. Bornschlegl, and U. Boesl, "Twin mass peak ion source for comparative mass spectrometry: Application to circular dichroism laser MS," *Int. J. Mass Spectrom.* **281**, 134–139 (2009).
- <sup>28</sup>A. Bornschlegl, C. Logé, and U. Boesl, "Investigation of CD effects in the multi-photon ionisation of R-(+)-3-methylcyclopentanone," *Chem. Phys. Lett.* **447**, 187–191 (2007).
- <sup>29</sup>H. G. Breunig, G. Urbasch, P. Horsch, J. Cordes, U. Koert, and K.-M. Weitzel, "Circular dichroism in ion yields of femtosecond-laser mass spectrometry," *ChemPhysChem* **10**, 1199–1202 (2009).
- <sup>30</sup>H. P. J. M. Dekkers and L. E. Cross, "The optical activity of low-symmetry ketones in absorption and emission," *J. Am. Chem. Soc.* **98**, 2210–2219 (1976).
- <sup>31</sup>J. Lepelmeier, J. L. Alonso-Gómez, F. Mortaheb, U. Boesl, U. Heiz, and A. Kartouzian, "Chiroptical inversion for isolated vibronic transitions of supersonic beam-cooled molecules," *Phys. Chem. Chem. Phys.* **19**, 21297 (2017).
- <sup>32</sup>F. Santoro, F. Mortaheb, J. Lepelmeier, U. Boesl, U. Heiz, and A. Kartouzian, "High-resolution absorption and electronic circular dichroism spectra of (R)-(+)-1-phenylethanol. Confident interpretation based on the synergy between experiments and computations," *ChemPhysChem* **19**, 715–723 (2018).
- <sup>33</sup>A. Kastner, C. Lux, T. Ring, S. Züllighoven, C. Sarpe, A. Senftleben, and T. Baumert, "Enantiomeric excess sensitivity to below one percent by using femtosecond photoelectron circular dichroism," *ChemPhysChem* **17**, 1119–1122 (2016).
- <sup>34</sup>A. Comby, E. Bloch, C. M. M. Bond, D. Descamps, J. Miles, S. Petit, S. Rozen, J. B. Greenwood, V. Blanchet, and Y. Mairesse, "Real-time determination of enantiomeric and isomeric content using photoelectron elliptical dichroism," *Nat. Commun.* **9**, 5212 (2018).
- <sup>35</sup>P. Horsch, G. Urbasch, K.-M. Weitzel, and D. Kröner, "Circular dichroism in ion yields employing femtosecond laser ionization—the role of laser pulse duration," *Phys. Chem. Chem. Phys.* **13**, 2378–2386 (2011).
- <sup>36</sup>D. Kröner, "Laser-driven electron dynamics for circular dichroism in mass spectrometry: From one-photon excitations to multiphoton ionization," *Phys. Chem. Chem. Phys.* **17**, 19643–19655 (2015).
- <sup>37</sup>M. Wollenhaupt, V. Engel, and T. Baumert, "Femtosecond laser photoelectron spectroscopy on atoms and small molecules: Prototype studies in quantum control," *Annu. Rev. Phys. Chem.* **56**, 25–56 (2005).
- <sup>38</sup>M. Wollenhaupt and T. Baumert, "Ultrafast laser control of electron dynamics in atoms, molecules and solids," *Faraday Discuss.* **153**, 9–26 (2011).

# Supplementary information: Self-referencing circular dichroism ion yield measurements for improved statistics using femtosecond laser pulses

T. Ring, C. Witte, S. Vasudevan, S. Das, S. T. Ranecky, H. Lee, N. Ladda, A. Senftleben, H. Braun, and T. Baumert  
 Universität Kassel, Heinrich-Plett-Str. 40, 34132 Kassel, Germany

This supplementary information contains the calculation of  $g$  for racemic 3-MCP. We describe the procedure for the single-peak as well as the self-referencing twin-peak measurements and include the achiral correction. It is supposed to clarify the procedure and establish confidence in the statistics after achiral correction and self-referencing.

As shown in figure S1 two spectra for the two different quarter-wave-plate settings are evaluated. They contain the twin-peak signal of the chiral sample and of an achiral reference. Each spectrum represents the average of the signal from 1280 consecutive laser pulses. All anisotropies  $g$  are calculated from the integrated ion yields  $I_{lcp}$  and  $I_{rcp}$  according to equation S1:

$$g = 2 \cdot \frac{I_{lcp} - I_{rcp}}{I_{lcp} + I_{rcp}}. \quad (S1)$$

The single peak evaluation takes only the upper or only the lower focus into account. The change in helicity is realized via rotation of the quarter-wave-plate:

$$g^{up} = 2 \cdot \frac{I_{lcp}^{45} - I_{rcp}^{135}}{I_{lcp}^{45} + I_{rcp}^{135}} \quad \text{and} \quad g^{low} = 2 \cdot \frac{I_{lcp}^{135} - I_{rcp}^{45}}{I_{lcp}^{135} + I_{rcp}^{45}}. \quad (S2)$$

Per definition the anisotropy of the achiral reference substance is zero. Any deviation is due to experimental imperfections. Consequently, we subtract  $g_{ref}$  from the anisotropy of the sample  $g_{sam}$  to correct for systematic deviations:

$$g_{cor}^{up} = g_{sam}^{up} - g_{ref}^{up} \quad \text{and} \quad g_{cor}^{low} = g_{sam}^{low} - g_{ref}^{low}. \quad (S3)$$

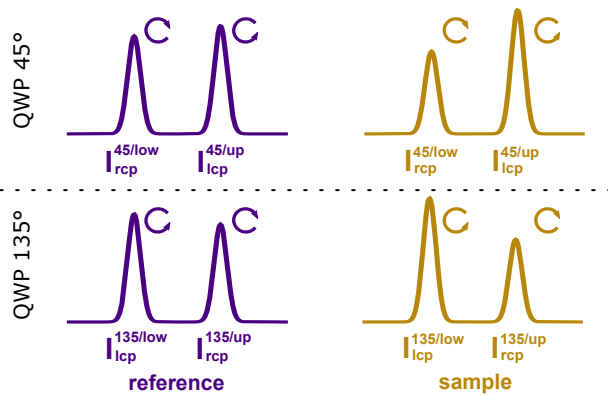


FIG. S1. Schematic outline of a mass spectrum for CD evaluation. Depicted are two spectra, the top one corresponds to a quarter-wave-plate angle of  $45^\circ$  and the bottom one to an angle of  $135^\circ$ . Each of them contains four mass peaks, the twin-peak of the achiral reference and the twin-peak of the chiral sample. The left peaks of each twin-pair stem from ionization in the lower focus and the right one from ionization in the upper focus. The helicity of the laser polarization is shown on top of the individual peaks.

In case of the twin-peak measurement all anisotropies can be calculated from one spectrum with a fixed quarter-wave-plate position:

$$g^{45} = 2 \cdot \frac{I_{lcp}^{up} - I_{rcp}^{low}}{I_{lcp}^{up} + I_{rcp}^{low}} \quad \text{and} \quad g^{135} = 2 \cdot \frac{I_{lcp}^{low} - I_{rcp}^{up}}{I_{lcp}^{low} + I_{rcp}^{up}}. \quad (S4)$$

Of course, this allows for achiral correction in the same way:

$$g_{cor}^{45} = g_{sam}^{45} - g_{ref}^{45} \quad \text{and} \quad g_{cor}^{135} = g_{sam}^{135} - g_{ref}^{135}. \quad (S5)$$

The average of both values delivers the reference corrected twin-peak anisotropy

$$g_{cor}^{twin} = \frac{g_{cor}^{45} + g_{cor}^{135}}{2}. \quad (S6)$$

Typically we perform 500 measurement cycles to get a robust statistic. The final anisotropy is the arithmetic mean

$$\bar{g} = \frac{1}{500} \cdot \sum_{i=1}^{500} g_i \quad (S7)$$

and the statistical error  $\delta\bar{g}$  is derived as three times the standard deviation of the mean  $\bar{\sigma}$

$$\delta\bar{g} = 3 \cdot \bar{\sigma} = \frac{3}{\sqrt{500}} \cdot \sqrt{\frac{1}{500-1} \cdot \sum_{i=1}^{500} (g_i - \bar{g})^2} \quad (S8)$$

The anisotropy should be zero within the scope of the measurement error for racemic 3-MCP. This is not the case for the uncorrected single-peak evaluation:

$$\bar{g}^{up} = (7.3 \pm 1.7) \% \quad \text{and} \quad \bar{g}^{low} = (6.2 \pm 1.7) \%. \quad (S9)$$

After correction with the achiral reference potassium the absolute values are smaller but still not zero:

$$\bar{g}_{cor}^{up} = (-2.3 \pm 1.1) \% \quad \text{and} \quad \bar{g}_{cor}^{low} = (1.9 \pm 1.1) \%. \quad (S10)$$

The twin-peak anisotropy finally yields the desired result:

$$\bar{g}_{cor}^{twin} = (-0.2 \pm 0.6) \%. \quad (S11)$$

The increase in reliability of this measurement and evaluation procedure is visualized in figure S11.

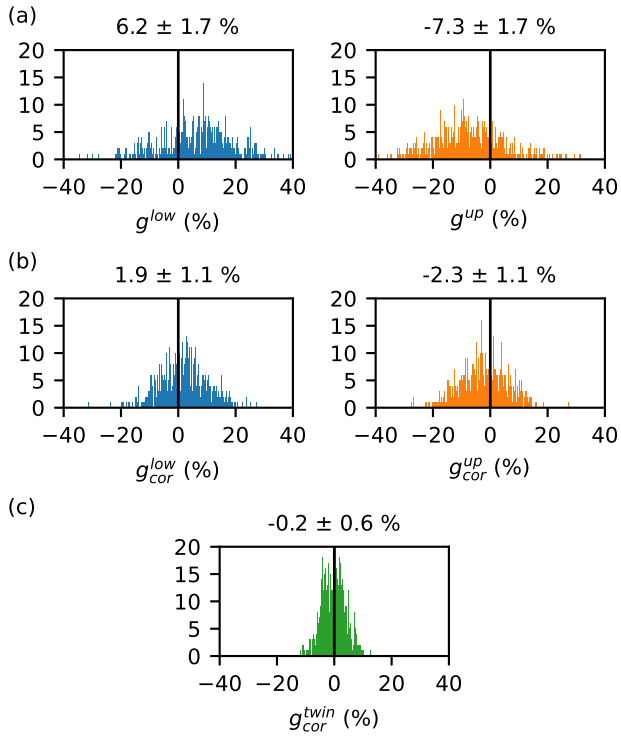


FIG. S11. Statistic distribution of the anisotropy of 3-MCP at 309 nm. Individual measurements according to figure 3(b) in the main manuscript: (a) single focus evaluation, (b) single focus evaluation with potassium correction, (c) reference corrected twin peak evaluation.